Entropic Penalty Switches Li^+ Solvation Site Formation and Transport Mechanisms in Mixed Polarity Copolymer Electrolytes

Supporting Information

Authors

Chuting Deng[1], Peter Bennington[1], Regina J. Sánchez-Leija[1], Shrayesh N. Patel[1,2], Paul F. Nealey[1,2,3], Juan J. de Pablo[1,2,3*]

Affiliations

[1] Pritzker School of Molecular Engineering, University of Chicago, 5640 S Ellis Ave, Chicago, IL 60637, United States

[2] Center for Molecular Engineering, Argonne National Laboratory, 9700 South Cass Avenue, Lemont, IL 60439, United States

[3] Materials Science Division, Argonne National Laboratory, 9700 South Cass Avenue, Lemont, IL 60439, United States

[*] depablo@uchicago.edu

Contents:

1 Methods and Force Field Parameters for Molecular Dynamics Simulations

In this study, the TraPPE-UA force field[1–3] is used for all inter- and intramolecular interactions between polymer atoms. Instead of rigid bonds used in the TraPPE-UA force field, the generalized CHARMM bonding spring constants are used[4]. Partial charges of the polymer interaction sites are refined through *ab initio* calculations using the B3LYP functional and the 6-31G(d,p) basis set, performed with GAUSSIAN 09 program[5]. The charge fitting uses the ChElPG calculation scheme[6]. Compatible all-atom parameters for LiTFSI are adapted from a previous simulation study[7,8]. An additional charge scaling of 0.7 is applied to Li^+ and $TFSI^-$[9]. Figure S1 provides reference labels for polymer atom types used in the force field.

The simulations were performed using the LAMMPS package[10]. For all MD simulations, a cutoff radius of 12 Å with Van der Waals tail correction was used for short-range Lennard-Jones (LJ) interactions. Long-range non-bonded interactions were cut off at a radius of 12 Å and were handled using the Particle-particle particle-mesh solver with 10^{-4} accuracy[11]. The trajectories were integrated using the velocity-Verlet algorithm with a 1 fs timestep. For NVT simulations, the Nosé-Hoover thermostat with a damping parameter of 100 fs was used. For NPT simulations, the Nosé-Hoover barostat with a damping parameter of 1000 fs was applied in addition to the thermostat.

1.1 United Atom Model: Terminal Groups, Tacticity, and Atom Type Assignments

The numbers of chains and numbers of repeat units for each system are summarized in **Table S1**. The salt concentration for all simulations is $r = [Li^+]/([EO]+[OCOO]) = 0.05$, where [OCOO] refers to the carbonyl oxygen in the cyclic carbonate group. The termini for the polymethacrylate backbone are CH3, which are connected to the CT interaction sites. All polymer chains in this study are atactic. When generating the initial configuration, the stereochemistry of each chiral center is randomly chosen as S or R with equal probability.

Table S1. Summary table of POEM homopolymer, PGCMA-*r*-POEM, and PGCMA-*b*-POEM simulation systems: system composition, polymer chain lengths, and fictive temperature.

System	Number of Chains	Number of Repeat Units	POEM wt.%	T_f
POEM	1 POEM	300	100	239 ± 5 K
PGCMA-*r*-POEM	1 PGCMA-*r*-POEM	432 (PGCMA)-*r*-168 (POEM)	50.3	276 ± 4 K
PGCMA-*b*-POEM	16 PGCMA-*b*-POEM	26 (PGCMA)-*b*-10 (POEM)	50.6	274 ± 3 K

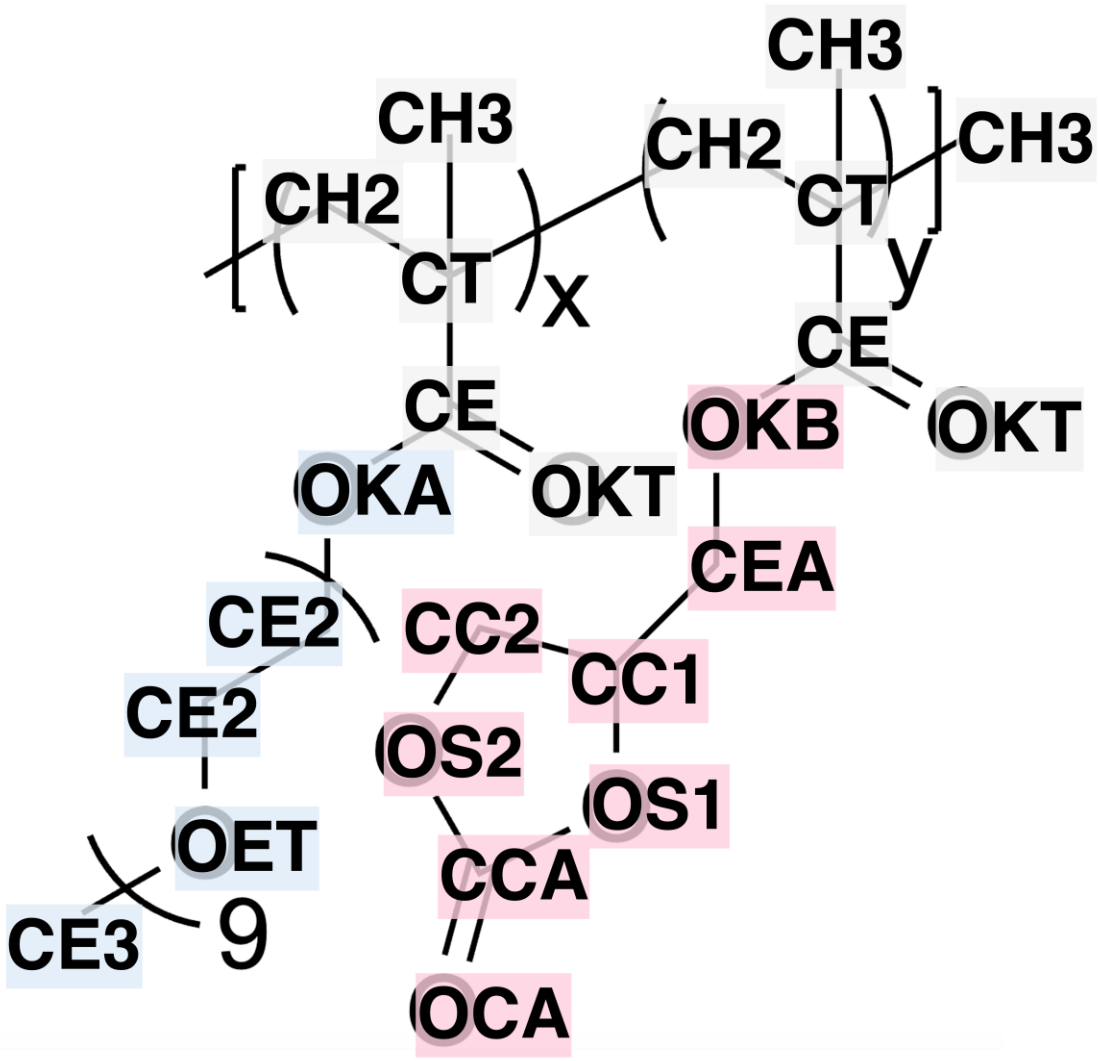

Figure S1. Reference labels for atom types in force field parameters.

1.2 Non-bonded Interaction Parameters

The nonbonded interactions include Lennard-Jones interactions and Coulombic interactions. For united atoms i and j, their nonbonded interaction is:

$$u_{nb}(r_{ij}) = 4\varepsilon_{ij}\left[\left(\frac{\sigma_{ij}}{r_{ij}}\right)^{12} - \left(\frac{\sigma_{ij}}{r_{ij}}\right)^{6}\right] + \frac{q_i q_j}{4\pi\epsilon_0 r_{ij}}, \quad (1)$$

where r_{ij} is the separation distance between atoms i and j, σ_{ij} is the Lennard-Jones diameter, ε_{ij} is the Lennard-Jones interaction strength, ϵ_0 is the vacuum permittivity. q_i and q_j are the partial charges of atoms i and j.

LJ interactions are computed with Lorentz-Berthelot mixing rules. For 1-2, 1-3, and 1-4 bonded interaction sites, the Lennard-Jones interactions are turned off. Coulomb interactions are turned off for 1-2 and 1-3 bonded interaction sites and scaled by 0.5 for 1-4 bonded interactions. The non-bonded interaction parameters are listed in table S2. The partial charges on chain termini are slightly adjusted to ensure charge neutrality.

Table S2: Nonbonded interaction potential parameters for polymer atoms.

atom	m (amu)	σ_{ii} (Å)	ϵ_{ii} ($\frac{\text{kcal}}{\text{mol}}$)	q (e)
CH2	14.027	3.95	0.091411	-0.0765
CH3	15.035	3.75	0.194746	-0.066
CT	12.011	6.4	0.000994	0.1826
CE	12.011	3.82	0.079488	0.6593
OKT	15.9994	3.05	0.156989	-0.514
OKA	15.9994	2.8	0.109296	-0.435
OET	15.9994	2.85	0.109296	-0.4757
CE2	14.027	3.95	0.091411	0.2413
CE3	15.035	3.75	0.194746	0.1875
OKB	15.9994	2.8	0.109296	-0.2887
CEA	14.027	3.95	0.091411	0.1015
CC1	13.019	4.33	0.01987	0.2193

CC2	14.027	3.95	0.091411	0.3004
OS1	15.9994	2.85	0.109296	-0.4153
OS2	15.9994	2.85	0.109296	-0.424
OCA	15.9994	3.05	0.156989	-0.5105
CCA	12.011	3.75	0.105	0.8319

1.3 Bonding Potential Parameters

1-2 bonded united atoms interact via a harmonic bonding potential in the form:

$$u_{bond}(r_{ij}) = k_{bond}\left(r_{ij} - {r_{ij}}^{(0)}\right)^2, \quad (2)$$

Where r_{ij} is the separation distance between atoms i and j, k_{bond} is the force constant and ${r_{ij}}^{(0)}$ is the equilibrium bond length. The bonding interaction parameters are listed in table S3.

Table S3: Bonding potential parameters for polymer atoms.

bond	k_{bond} ($\frac{\text{kcal}}{\text{mol}\cdot\text{Å}^2}$)	${r_{ij}}^{(0)}$ (Å)	bond	k_{bond} ($\frac{\text{kcal}}{\text{mol}\cdot\text{Å}^2}$)	${r_{ij}}^{(0)}$ (Å)
CE2-CE2	225	1.540	CH2-CH2	225	1.540
CE2-OET	360	1.410	OCA-CCA	360	1.229
CE3-OET	360	1.410	CCA-OS1	360	1.344
CH3-CT	225	1.540	CCA-OS2	360	1.344
CH2-CT	225	1.540	OS1-CC1	360	1.410
CEA-OKB	360	1.410	OS2-CC2	360	1.410
CE2-OKA	360	1.410	CC2-CC1	225	1.540
CE-CT	200	1.520	CC1-CEA	225	1.540
CE-OKT	360	1.200	CE-OKB	360	1.344
CE-OKA	360	1.344			

1.4 Bending Potential Parameters

1-2-3 bonded united atoms interact via a harmonic bending potential in the form:

$$u_{bend}(\theta_{ijk}) = k_{bend}(\theta_{ijk} - {\theta_{ijk}}^{(0)})^2, \quad (3)$$

Where k_{bend} is the force constant, θ_{ijk} is the angle between united atoms i, j, and k, and ${\theta_{ijk}}^{(0)}$ is the equilibrium angle. The bending interaction parameters are listed in table S4.

Table S4: Bending potential parameters for polymer atoms.

bend	k_{bend} ($\frac{\text{kcal}}{\text{mol·rad}^2}$)	${\theta_{ijk}}^{(0)}$ (Å)	bend	k_{bend} ($\frac{\text{kcal}}{\text{mol·rad}^2}$)	${\theta_{ijk}}^{(0)}$ (Å)
CE2-OET-CE2	60.0136	112.0	CH3-CT-CH3	62.1000	109.5
CE2-OET-CE3	60.0136	112.0	OKA-CE2-CE2	49.9782	112.0
CE2-CE2-OET	49.9782	112.0	OKB-CEA-CC1	49.9782	112.0
CH2-CT-CH2	62.1000	109.5	OCA-CCA-OS1	40.0600	123.0
CH3-CT-CH2	62.1000	109.5	OCA-CCA-OS2	40.0600	123.0
CT-CH2-CT	62.1000	114.0	CCA-OS2-CC2	62.1000	115.0
CE-OKB-CEA	62.1000	115.0	CCA-OS1-CC1	62.1000	115.0
CE-OKA-CE2	62.1000	115.0	OS1-CCA-OS2	72.4000	110.0
OKT-CE-OKA	62.1000	125.0	OS2-CC2-CC1	59.9400	112.0
OKT-CE2-C2	49.9782	112.0	OS1-CC1-CC2	59.9400	112.0
CH2-CT-CE	62.1000	109.5	OS1-CC1-CEA	59.9400	112.0
CT-CE-OKT	62.1000	125.0	CC2-CC1-CEA	62.1000	112.0
CT-CE-OKA	70.1483	110.0	OKT-CE-OKB	62.1000	125.0
CH3-CT-CE	62.1000	109.5	CT-CE-OKB	70.1483	110.0

1.5 Torsional Potential Parameters

The torsional potentials for 1-2-3-4 bonded united atoms take the form:

$$u_{tors}(\phi_{ijkl}) = \frac{K_1}{2}\left[1 + \cos(\phi_{ijkl})\right] + \frac{K_2}{2}\left[1 - \cos(2\phi_{ijkl})\right] + \frac{K_3}{2}\left[1 + \cos(3\phi_{ijkl})\right] + \frac{K_4}{2}\left[1 - \cos(4\phi_{ijkl})\right], \quad (4)$$

Where c_1, c_2, and c_3 are coefficients and ϕ_{ijkl} is the dihedral angle defined by atoms i, j, k, and l. The torsional interaction parameters are listed in table S5.

Table S5: Torsional potential parameters for polymer atoms.

torsion	K_1 ($\frac{\text{kcal}}{\text{mol}}$)	K_2 ($\frac{\text{kcal}}{\text{mol}}$)	K_3 ($\frac{\text{kcal}}{\text{mol}}$)	K_4 ($\frac{\text{kcal}}{\text{mol}}$)
OKA-CE2-CE2-OET	1.888000	-1.888000	0.000000	0.000000
OET-CE2-CE2-OET	1.888000	-1.888000	0.000000	0.000000
CE2-CE2-OET-CE2	2.882840	-0.650809	2.218510	0.000000
CE2-CE2-OET-CE3	2.882840	-0.650809	2.218510	0.000000
CH3-CT-CH2-CT	0.000000	0.000000	1.833350	0.000000
CH2-CT-CH2-CT	0.000000	0.000000	1.833350	0.000000
CT-CH2-CT-CE	0.000000	0.000000	1.833350	0.000000
CH3-CT-CE-OKT	-0.919280	0.229880	-0.609280	0.000000
CH2-CT-CE-OKT	-0.919280	0.229880	-0.609280	0.000000
CH3-CT-CE-OKA	0.915310	0.216840	0.609670	0.000000
CH2-CT-CE-OKA	0.915310	0.216840	0.609670	0.000000
CT-CE-OKB-CEA	9.689610	7.678560	1.387070	0.000000
CT-CE-OKA-CE2	9.689610	7.678560	1.387070	0.000000
CE-OKA-CE2-CE2	-2.988080	2.142010	-0.087834	0.203768
OKT-CE-OKB-CEA	-9.669740	7.376500	-1.045270	0.000000
OKT-CE-OKA-CE2	-9.669740	7.376500	-1.045270	0.000000
OCA-CCA-OS2-CC2	-0.636000	6.488000	0.870000	0.000000
OCA-CCA-OS1-CC1	-0.636000	6.488000	0.870000	0.000000
CCA-OS2-CC2-CC1	-0.404000	4.748000	2.418000	0.000000

CCA-OS1-CC1-CC2	-0.404000	4.748000	2.418000	0.000000
OS1-CCA-OS2-CC2	0.000000	9.000000	0.000000	0.000000
OS2-CCA-OS1-CC1	0.000000	9.000000	0.000000	0.000000
OS2-CC2-CC1-OS1	0.574000	-0.422000	4.562000	0.000000
OS2-CC2-CC1-CEA	0.702000	-0.212000	3.060000	0.000000
CE-OKB-CEA-CC1	-2.988080	2.142010	-0.087834	0.203768
OKB-CEA-CC1-OS1	1.888000	-1.888000	0.000000	0.000000
CCA-OS1-CC1-CEA	-0.404000	4.748000	2.418000	0.000000
CC2-CC1-CEA-OKB	0.702000	-0.212000	3.060000	0.000000
CH3-CT-CE-OKB	0.915310	0.216840	0.609670	0.000000
CH2-CT-CE-OKB	0.915310	0.216840	0.609670	0.000000

2 Simulation Protocol

To prepare the starting configuration, the polymer chains are initiated with random positions and orientations in a large box. The polymer chains are first relaxed under the NVT ensemble at 500 K for 30 ns. Then a 40 ns NPT equilibration at 500 K and 1 bar is performed for polymer chains to equilibrate and to ensure the bulk density does not drift. The process of introduction of Li^+ is as follows: Li^+ and $TFSI^-$ ions are introduced at random positions in the equilibrated neat polymer at the designated ratio of $r = 0.05$. To remove any steric clashes in the simulation cell, the system is relaxed under the NVE ensemble for 10,000 steps, where the maximum displacement of an atom is limited to 0.1 Å per step.

To perform each production simulation, the salt-doped polymer is equilibrated at the designated temperature under the NPT ensemble for 40 ns. Then the system is further equilibrated for 10 ns under the NVT ensemble. At the beginning of this NVT equilibration, the box size is scaled to reflect the ensemble average density during the last 10 ns of the NPT equilibration. Then, the trajectory for analysis is collected from a 150-ns production simulation under the NVT ensemble.

3 Fictive Temperature Determination

To determine the fictive temperature, equilibrated configurations at a high temperature are continuously cooled at a cooling rate of 10 K/ns at 1 bar. For POEM, the system is cooled from 400 K to 50 K. For PGCMA-*r*-POEM and PGCMA-*b*-POEM, the system is cooled from 500 K to 50 K. The density is plotted as a function of temperature under the NPT ensemble. Two linear segments are fitted for the glass and liquid regions respectively. The T_f is determined as the intercept of the extrapolated linear fit lines. This procedure to calculate T_f is sensitive to the fitting range of the two segments. Therefore, the endpoints of the fitting segments are systematically sampled in the following manner. The starting point of the glassy segment was fixed at 50 K, while the endpoint of the glassy segment was randomly sampled between 100 K and 150 K. Similarly, the starting point of the liquid segment was fixed at the starting temperature, 400 K and 500 K for POEM and the copolymers, respectively. The endpoint of the liquid segment was sampled between 300 K and 350 K for POEM. For the copolymers, the endpoint of the liquid segment was sampled between 350 K and 400 K. The fitting intervals for the glassy segment and the liquid segment are randomly drawn within the sampling interval defined above, the intersections between which yield a set of T_f values. Only T_f values that fall between the endpoints of fitting segments are kept. The T_f calculation described above was repeated for another independent sample. For each sample, combinations of glassy and liquid fitting ranges are generated 10,000 times. The mean and standard deviation of the set of T_f values collected from both samples are reported. Figure S4 includes the cooling curve and the distribution of resulting T_f values collected.

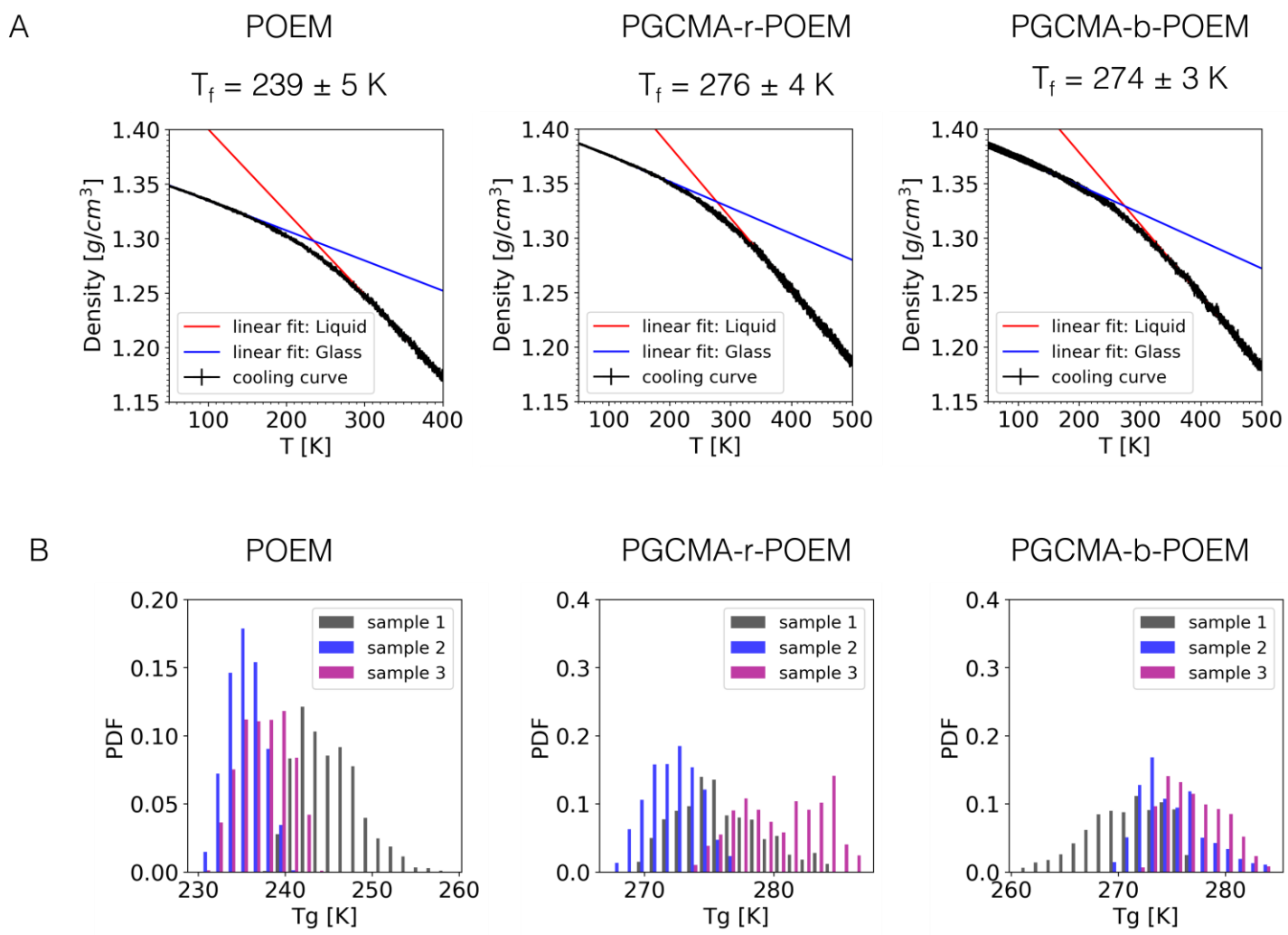

Figure S2. Fictive temperatures in simulations. (A) Density as a function of temperature for POEM homopolymer, PGCMA-*r*-POEM, and PGCMA-*b*-POEM copolymers, respectively. Example fitting lines for liquid and glassy regions are shown in red and blue, respectively. The error bars of the cooling curve arise from three independent runs. (B) Normalized histograms of collected T_f values. Histograms from three independent samples are plotted in different colors.

4 Calculation of Functional Group Dipole Moments

The dipole moments of the cyclic carbonate fragment and the C-O-C ethylene oxide fragment are obtained based on the following geometry:

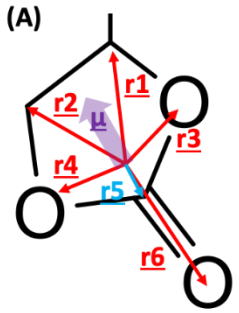

Average distance r_i from center of mass [Å]	
r1	1.57
r2	1.60
r3	1.13
r4	1.10
r5	0.72
r6	1.93

Average Angle between r_i and μ	
r1	32°
r2	26°
r3	90°
r4	84°
r5	169°
r6	175°

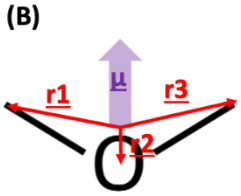

Average distance r_i from center of mass [Å]	
r1	1.20
r2	0.51
r3	1.20

Average Angle between r_i and μ	
r1	76°
r2	180°
r3	76°

Figure S3: (A) Average geometry for a GCMA fragment. (B) Average geometry for a C-O-C fragment along the POEM side chain. The results are obtained from MD simulation at 150K above T_f and are found to be independent of temperature.

5 Calculation of Dielectric Constant

The dielectric constant ε is computed based on the fluctuation of permanent dipole (Eq. 5),

$$\varepsilon = 1 + \frac{4\pi[\langle \boldsymbol{M}^2 \rangle - \langle \boldsymbol{M} \rangle^2]}{3kTV} \tag{5}$$

Where k is Boltzmann's constant, T is temperature, V is the box volume. The ensemble averages are defined as

$$\langle \boldsymbol{M}^2 \rangle = \frac{1}{N_s}\sum_{i=1}^{N_s} \boldsymbol{M}^2(t_i) \quad \text{and} \quad \langle \boldsymbol{M} \rangle^2 = \left[\frac{1}{N_s}\sum_{i=1}^{N_s} \boldsymbol{M}(t_i)\right]^2. \tag{6}$$

Where $\boldsymbol{M}(t) = \frac{e}{\sqrt{4\pi\epsilon_0}}\sum_{i=1}^{N} z_i \boldsymbol{r}_i(t)$ is the instantaneous dipole moment at time t. To correctly compute ε, no bonded atoms are allowed to cross the periodic boundary. This means that the molecules are unwrapped and made "whole", and their centers of mass are contained in the {0,0,0} box image.

6 Effects of Alternative Partial Charge Assignment on Li^+ Coordination

To test the robustness of the entropy argument on the Li^+ solvation trend, two sets of additional simulations were performed, where the partial charges are assigned based on different rationales, and all other parameters are kept identical. The original model used for the rest of the work is referred to as model 1. In model 2, the partial charges for Li^+ and $TFSI^-$ from ref. [7] are used as-is without rescaling. In model 3, the polymer partial charges are adapted directly from ref.[3,12] for POEM and ref.[13] for PGCMA. The partial charges for Li^+ and $TFSI^-$ in model 3 are unscaled. Table S6 lists the partial charges on the polymer interaction sites adapted from ref.[3,12]. The readers are referred to the original work for parameters of Li^+ and $TFSI^-$.

Table S6: Partial charges assigned on polymer interaction sites in model 3. The partial charges on chain termini are slightly adjusted to ensure charge neutrality.

atom	$q\ (e)$	atom	$q\ (e)$
CH2	0.00	OKB	-0.40
CH3	0.00	CEA	0.25
CT	0.00	CC1	0.2227
CE	0.55	CC2	0.229
OKT	-0.45	OS1	-0.4314
OKA	-0.40	OS2	-0.4314
OET	-0.50	OCA	-0.6378
CE2	0.25	CCA	1.0489
CE3	0.25		

The three models cover all possible cases of relative polarity among the three competing Li^+-solvating units: O(ether), O=(carbonate), and O(TFSI). While O=(carbonate) stays more polar than O(ether) in all three models, the polarity of O(TFSI), relative to the other two oxygen types, ranks as lowest in model 1, highest in model 2, and between them in model 3. To probe the Li^+ solvation environment under models 2 and 3, radial distribution functions and coordination numbers shown in Figure 4 are replicated below using the alternative models. Since

the three models only differ in the partial charges, the size of the solvation shell varies minimally across them. Consistent with Figure 4, the first solvation shell is comprised of O(ether), O=(carbonate), and O(TFSI), whereas O(ester) and O(carbonyl) from the backbone, despite being more polar than O(ether) are absent. Similar to the findings from Figure 4, Figure S3 shows that the relative contribution to Li^+ first solvation shell from O(TFSI) and O=(carbonate) relates closely to their polarity rank. Such polarity argument again does not apply to O(ether), which is always the predominant Li^+-solvating unit regardless of the polarity rank. Figure 4 and S3 combine to reinforce that while the polarity argument is generally applicable, it is not sufficient to describe the preferential Li^+ solvation by O(ether).

Model 2

A

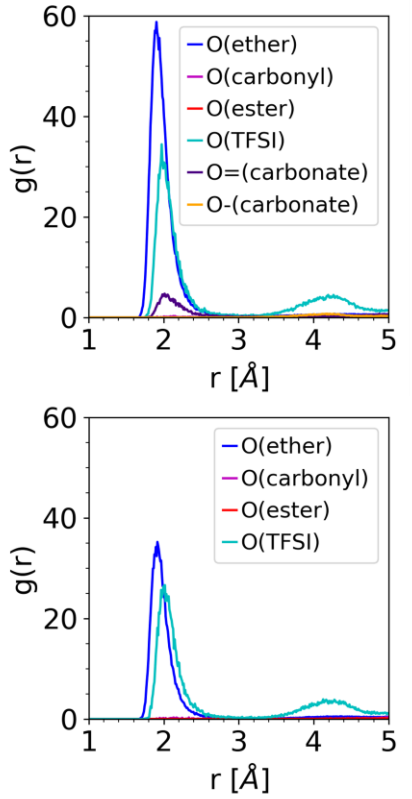

B

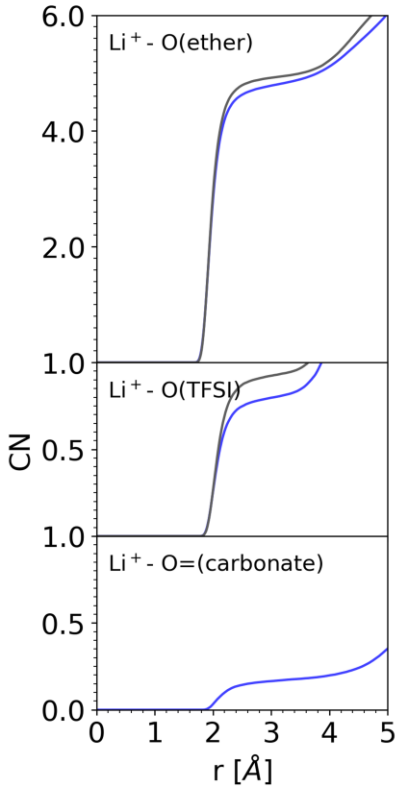

Model 3

C

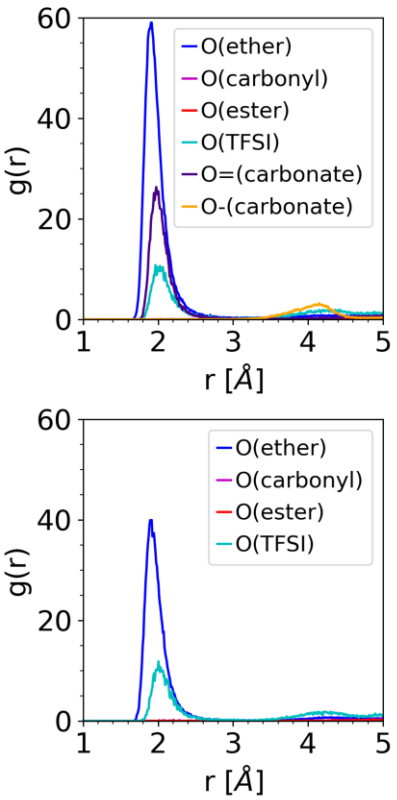

D

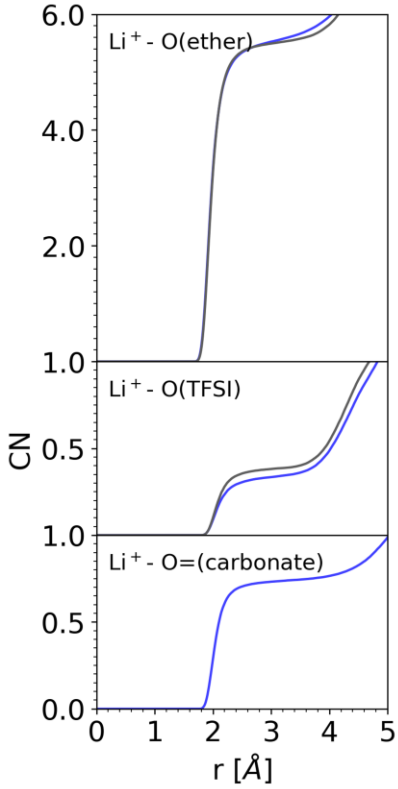

Figure S4: (A, C) Radial distribution functions between Li^+ and oxygen atoms in POEM (top) and PGCMA-*r*-POEM (bottom). (B, D) Coordination numbers CNij(r) in POEM and PGCMA-*r*-POEM between Li^+ and O(ether) (top), O(TFSI) (center), and O=(carbonate) (bottom). The results are obtained at 150 K above Tf using (A-B) model 2 and (C-D) model 3.

7 Degrees of Independent Ion Motions in POEM and in PGCMA-r-POEM

The degree of independent ion motions, α, is defined as the ratio of correlated MSD to the self MSD (Eq. 7). In a simulation, obtaining long-time valid statistics for α is often difficult, so the value of α is commonly estimated over the sub-diffusive regime at short timescales and extrapolated to longer timescales[14,15]. Here we compute α as a function of time and report the averaged value over the first 10 ns.

$$\alpha = \lim_{t\to\infty} \frac{\sum_{i=1}^{N_{ion}} \sum_{j=1}^{N_{ion}} z_i z_j \langle [\boldsymbol{r}_i(t) - \boldsymbol{r}_i(0)] \cdot [\boldsymbol{r}_j(t) - \boldsymbol{r}_j(0)] \rangle}{\sum_{i=1}^{N_{ion}} z_i^2 \langle \|\boldsymbol{r}_i(t) - \boldsymbol{r}_i(0)\|^2 \rangle} \tag{7}$$

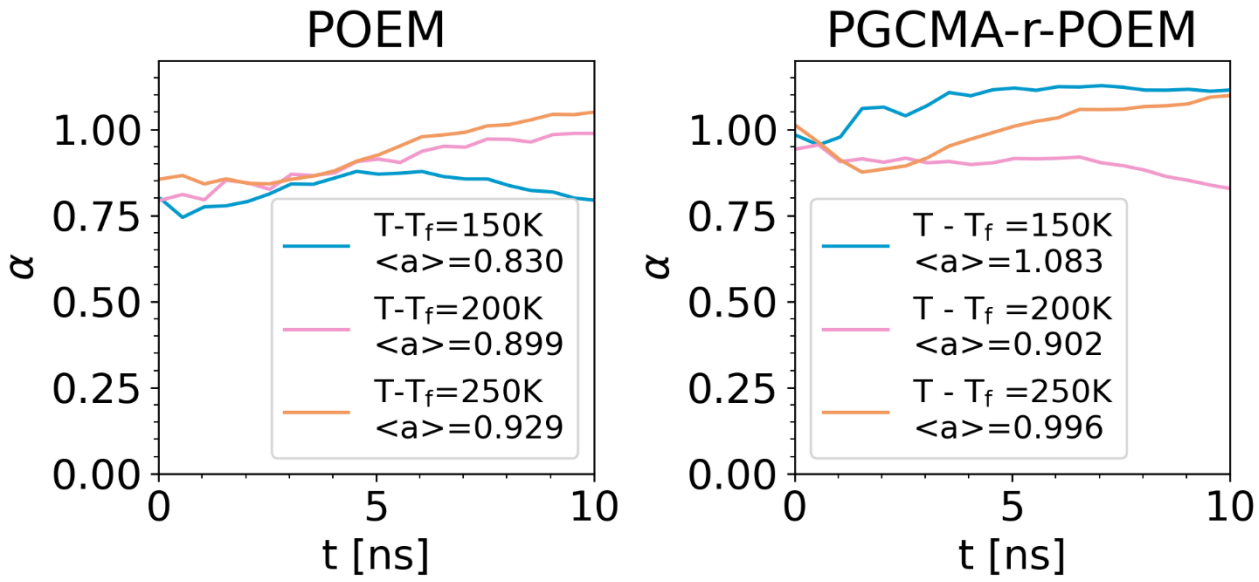

Figure S5: α as a function of correlation time for POEM and PGCMA-r-POEM. The averaged values for α are reported in the legend accordingly. The results show that ion motions are reasonably uncorrelated in both materials under the simulation conditions.

8 Binding Probability of O(ether) to Li^+ Along POEM Side Chains in POEM and PGCMA-*r*-POEM

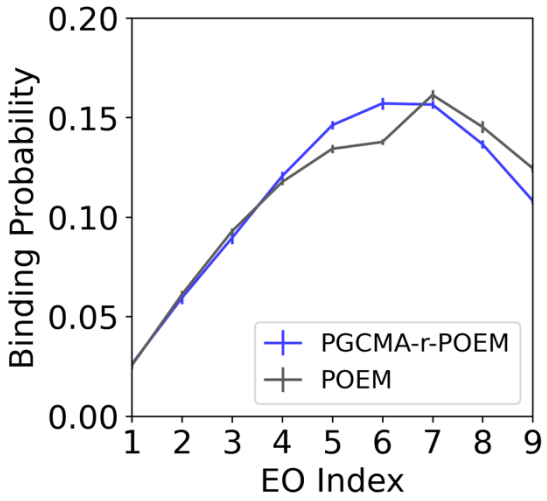

Fig. S6. Binding probability of O(ether) to Li^+ as a function of the position along a POEM side chain. The trends in the two materials are highly similar. Li^+ are found to be primarily solvated by O(ether) at positions 4-8 along the side chain. The side chains are split into five independent sets to obtain estimates of error.

9 Decay of Effective Concentration in PGCMA-*r*-POEM and PGCMA-*b*-POEM

To demonstrate the degree of miscibility, we probe the interchain packing of POEM in PGCMA-b-POEM (BCP) versus in PGCMA-*r*-POEM (RCP) in terms of the decay of effective concentration. As described in ref. [16] and [17], the normalized effective concentration of a component decays from unity to zero and indicates how closely a chain packs with other chains of the same species. The plot shows that the normalized effective concentration of POEM decays faster in the RCP, revealing a higher degree of intermixing in the RCP.

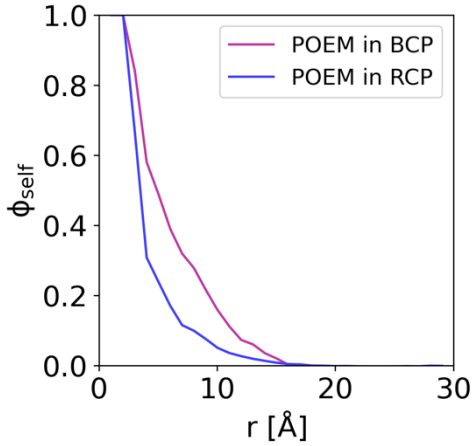

Fig. S7. Normalized decay of the self-effective concentration of the POEM component in PGCMA-*r*-POEM and PGCMA-*b*-POEM.

10 Population of Coordination Motifs in PGCMA-*b*-POEM

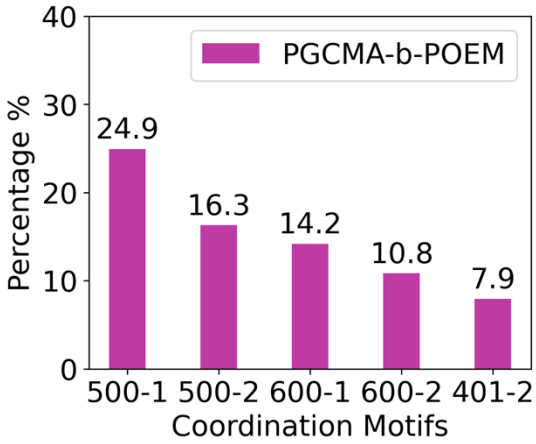

Fig. S8. Population of five most abundant Li^+ coordination motifs in PGCMA-*b*-POEM at T- T_f = 150 K. The plot uses the identical notation rule for coordination motifs as for PGCMA-*r*-POEM, as described in Figure 5.

References

(1) Martin, M. G.; Siepmann, J. I. Transferable Potentials for Phase Equilibria. 1. United-Atom Description of n-Alkanes. *Journal of Physical Chemistry B* **1998**, *102* (14), 2569–2577. https://doi.org/10.1021/jp972543+.

(2) Stubbs, J. M.; Potoff, J. J.; Siepmann, J. I. Transferable Potentials for Phase Equilibria. 6. United-Atom Description for Ethers, Glycols, Ketones, and Aldehydes. *J Phys Chem B* **2004**, *108* (45), 17596–17605. https://doi.org/10.1021/jp049459w.

(3) Maerzke, K. A.; Schultz, N. E.; Ross, R. B.; Siepmann, J. I. TraPPE-UA Force Field for Acrylates and Monte Carlo Simulations for Their Mixtures with Alkanes and Alcohols. *J Phys Chem B* **2009**, *113* (18), 6415–6425. https://doi.org/10.1021/jp810558v.

(4) Vanommeslaeghe, K.; Hatcher, E.; Acharya, C.; Kundu, S.; Zhong, S.; Shim, J.; Darian, E.; Guvench, O.; Lopes, P.; Vorobyov, I.; Mackerell, A. D. CHARMM General Force Field: A Force Field for Drug-like Molecules Compatible with the CHARMM All-Atom Additive Biological Force Fields. *J Comput Chem* **2010**, *31* (4), 671–690. https://doi.org/10.1002/jcc.21367.

(5) M. J. Frisch, G. W. Trucks, H. B. Schlegel, G. E. Scuseria, M. A. Robb, J. R. Cheeseman, G. Scalmani, V. Barone, G. A. Petersson, H. Nakatsuji, X. Li, M. Caricato, A. Marenich, J. Bloino, B. G. Janesko, R. Gomperts, B. Mennucci, H. P. Hratchian, J. V. Ort, and D. J. F. Gaussian 09, Revision A.02. Gaussian, Inc.: Wallingford CT 2016.

(6) Breneman, C. M.; Wiberg, K. B. Determining Atom-Centered Monopoles from Molecular Electrostatic Potentials. The Need for High Sampling Density in Formamide Conformational Analysis. *J Comput Chem* **1990**, *11* (3), 361–373. https://doi.org/10.1002/jcc.540110311.

(7) Lopes, N. C.; Pascal, B. Molecular Force Field for Ionic Liquids Composed of Triflate or Bistriflylimide Anions. *Journal of Chemical Physics B* **2004**, *108* (1), 16893–16898. https://doi.org/10.1021/jp0476545.

(8) Wu, H.; Wick, C. D. Computational Investigation on the Role of Plasticizers on Ion Conductivity in Poly(Ethylene Oxide) LiTFSI Electrolytes. *Macromolecules* **2010**, *43* (7), 3502–3510. https://doi.org/10.1021/ma902758w.

(9) Brooks, D. J.; Merinov, B. V.; Goddard, W. A.; Kozinsky, B.; Mailoa, J. Atomistic Description of Ionic Diffusion in PEO–LiTFSI: Effect of Temperature, Molecular Weight, and Ionic Concentration. *Macromolecules* **2018**, *51* (21), 8987–8995. https://doi.org/10.1021/acs.macromol.8b01753.

(10) Plimpton, S. Fast Parallel Algorithms for Short-Range Molecular Dynamics. *J Comput Phys* **1995**, *117* (1), 1–19. https://doi.org/10.1006/jcph.1995.1039.

(11) Brown, W. M.; Kohlmeyer, A.; Plimpton, S. J.; Tharrington, A. N. Implementing Molecular Dynamics on Hybrid High Performance Computers – Particle–Particle Particle-Mesh. *Comput Phys Commun* **2012**, *183* (3), 449–459. https://doi.org/10.1016/j.cpc.2011.10.012.

(12) Wick, C. D.; Theodorou, D. N. Connectivity-Altering Monte Carlo Simulations of the End Group Effects on Volumetric Properties for Poly(Ethylene Oxide). *Macromolecules* **2004**, *37* (18), 7026–7033. https://doi.org/10.1021/ma049193r.

(13) Soetens, J.-C.; Millot, C.; Maigret, B.; Bakó, I. Molecular Dynamics Simulation and X—Ray Diffraction Studies of Ethylene Carbonate, Propylene Carbonate and Dimethyl Carbonate in Liquid Phase. *J Mol Liq* **2001**, *92* (3), 201–216. https://doi.org/10.1016/S0167-7322(01)00192-1.

(14) Wheatle, B. K.; Keith, J. R.; Mogurampelly, S.; Lynd, N. A.; Ganesan, V. Influence of Dielectric Constant on Ionic Transport in Polyether-Based Electrolytes. *ACS Macro Lett* **2017**, *6* (12), 1362–1367. https://doi.org/10.1021/acsmacrolett.7b00810.

(15) Borodin, O.; Smith, G. D. Mechanism of Ion Transport in Amorphous Poly(Ethylene Oxide)/LiTFSI from Molecular Dynamics Simulations. *Macromolecules* **2006**, *39* (4), 1620–1629. https://doi.org/10.1021/ma052277v.

(16) Sharon, D.; Deng, C.; Bennington, P.; Webb, M. A.; Patel, S. N.; de Pablo, J. J.; Nealey, P. F. Critical Percolation Threshold for Solvation-Site Connectivity in Polymer Electrolyte Mixtures. *Macromolecules* **2022**, *55* (16), 7212–7221. https://doi.org/10.1021/acs.macromol.2c00988.

(17) Sacristan, J.; Chen, C.; Maranas, J. K. Role of Effective Composition on Dynamics of PEO-PMMA Blends. *Macromolecules* **2008**, *41* (14), 5466–5476. https://doi.org/10.1021/ma8003373.